Balancing of Common DC-Bus Parallel Connected Modular Inductive Power Transfer Systems

Hakan Polat, Enes Ayaz, Ogün Altun, Ozan Keysan

Abstract—The aim of this paper is to design a modular, fault tolerant multi transmitter(Tx) -multi receiver(Rx) parallel connected common DC bus inductive power transfer(IPT) system to replace slip rings in wind turbines or brushless exciters. In parallel connected common DC bus systems, current unbalance is a major issue which results in thermal stresses and over current or voltages. In this paper, two different new current balancing methods are proposed: Cross-coupled Rx modules and intentional miss-tuning of Rx side resonant frequency. These methods are investigated both analytically and experimentally for a single Tx and two Rx system for a 500 W prototype. The proposed methods are tested independently, and then the combined current balancing method is also investigated. For the same missalignment case cross-coupled/de-tuned has a 55.8% current balancing improvement compared to de-coupled/fully-tuned topology.

Index Terms—Wireless power transfer, inductive power transfer, modular design, common DC bus, current balancing

I. INTRODUCTION

Inductive power transfer (IPT) systems have become more popular in recent years [1]. They are used in wide range from low power applications to high power applications [2]. Cordless design and spatial flexibility of IPTs led them to be used in applications such as portable chargers [3], [4], biomedical implements [5], electric cars [6], etc. They also provide electrical safety and galvanic isolation which makes them suitable for extremely dirty or extremely clean environments. IPT systems also allow to use multiple transmitters (Tx) and receivers (Rx) [7]–[9]. Multiple Tx-Rx systems are investigated and analyzed for applications in the literature [10]–[12]. Multiple Tx coils are generally implemented to obtain higher power ratings and to achieve modularity where power rating can be adjusted according to demand. Multiple Rx coils can also be used to achieve higher power levels with lower semiconductor ratings. Connection of the Rx modules can be adjusted such that they are connected in parallel or series or each module may supply independent loads [13]. In the literature, power sharing between parallel Rx's, also known as load balancing, is considered to be challenging due to different Tx-Rx couplings. This problem is either solved by replacing passive rectifiers with active rectifiers [4], [14] and implementing control algorithm in the receiver side or

by applying post-regulation by an extra DC-DC converter (Buck, Boost, Buck-Boost, etc.) [15]. Although these solutions are viable for compensating large coupling differences for parallel connected Rx modules, they are more complex and require additional components, which increases the size and the cost of the overall system. This is unfeasible for size-limited applications such as portable chargers. For systems where the magnetic couplings are close to each other for multi Rx modules, it is best to eliminate the effect of small coupling differences which may arise due to manufacturing tolerances. Moreover, using passive diode rectifiers at the output decreases the cost and reduces the complexity of the overall system compared to using an extra DC-DC converter or active rectifier control algorithms. The aim of this paper, is to present two novel methods to reduce current unbalance of multiple Rx modules. The proposed methods increase the efficiency, decrease ohmic losses and thermal stress on the semiconductors without the need of active rectifiers or post-regulation. This reduces the size of the Rx modules.

In the first section, structure and parameters of the 1Tx-2Rx system will be introduced. Then, current unbalance problem will be described briefly and confirmed by simulations. In the next sections, effect of cross-coupling and intentional de-tuning of Rx side on the current sharing will be discussed. Proposed methods will be later proven experimentally.

II. SYSTEM STRUCTURE AND PARAMETERS

The proposed system which is presented in Fig. 1, consists of two Tx side and four Rx side modules. The aim is to design a contactless-slip ring which can be mounted directly around the rotating shaft. Since the Rx side rotates with the shaft, the airgap clearance stays constant during operation however, change in the magnetic coupling between Tx-Rx modules are inevitable. Series-series topology is selected since the resonant frequency is independent of coupling and electrical loading. To further increase the reliability a modular structure is selected [16], [17]. This way during a single Rx module open circuit fault, the power transfer without over-loading the Tx side is possible. Moreover, having modularity allows power scaling of the system where the system can be up-scaled by adding additional Tx and Rx modules or down-scaled by reducing Rx side modules. Although the aim is to design 2Tx-4Rx system with a common DC bus, in this paper, a single Tx and two Rx modules system is analyzed for simplicity. The 1Tx-2Rx system can be upscaled to a 2Tx-4Rx without extra analysis. The system parameters are listed in Table I. In Fig. 2, 1Tx-2Rx structure is presented. Full bridge converters are used in
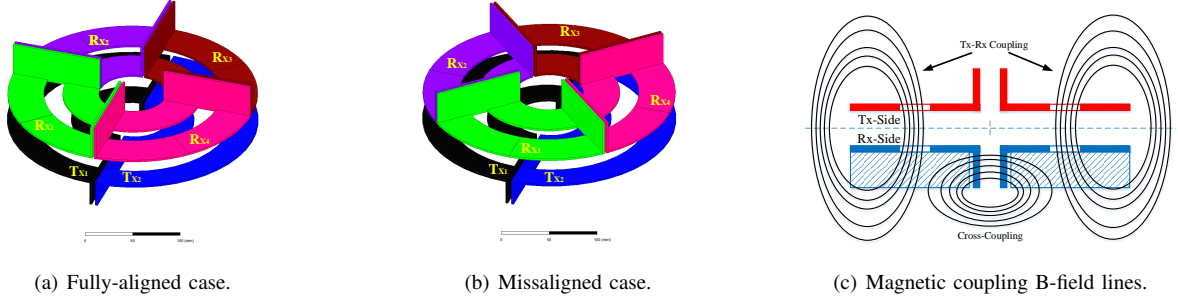
Corresponding Author: Ozan Keysan, keysan@metu.edu.tr

(a) Fully-aligned case.　　　(b) Missaligned case.　　　(c) Magnetic coupling B-field lines.

Fig. 1. (a)Fully-aligned position of IPT coils. (b)Miss-aligned position of IPT coils. (c)B-field line representation of magnetic coupling and cross-coupling.

the Tx side and full bridge passive diode rectifiers are used in the Rx side. The outputs of both Rx modules are connected in parallel.

TABLE I
SYSTEM PARAMETERS

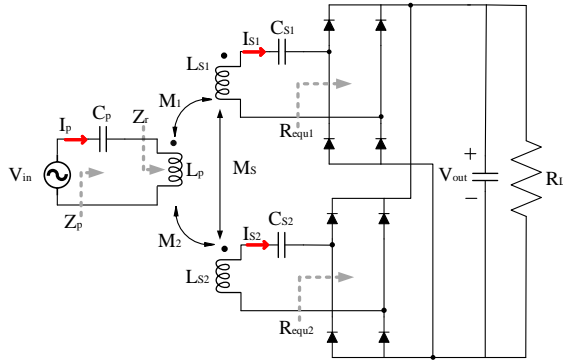| Parameters	Value
Power Rating	500 W
Input Voltage V_{in}	100 V
Output Voltage V_{out}	100 V
Resonant Frequency	150 kHz
Tx Inductance L_{Tx}	82 μH
Rx Inductance L_{Rx}	64 μH
Load Resistance R_{load}	20 Ω

Fig. 2. Parallel connected Rx's with common DC bus.

III. PROBLEM DEFINITION

In parallel connected Rx modules, maintaining equal current sharing between the modules is challenging as the module with higher magnetic coupling becomes the main power delivery path. The output voltage is set by the module with higher coupling and the rectifier diodes on the other module are blocked, which results in current and power unbalances. In Fig. 3, an initial simulation was performed to show this unbalanced condition. The initial system parameters are presented in Table I. At this stage the cross-coupling between the Rx modules is omitted and the resonant capacitors are adjusted such that both Tx and Rx sides are set to 150 kHz. The

operating frequency is set as 156 kHz to ensure an operation at the inductive region which guarentees zero voltage switching at power MosFET's of the Tx side. In Fig 3, two cases are presented where both Rx coils are fully-aligned with the Tx coil (i.e. both magnetic couplings are the identical). However, for the missaligned case , in which the magnetic couplings are different, the output voltages for both modules are same but the current sharing is clearly not equal in different coupling case as shown in Fig. 3.
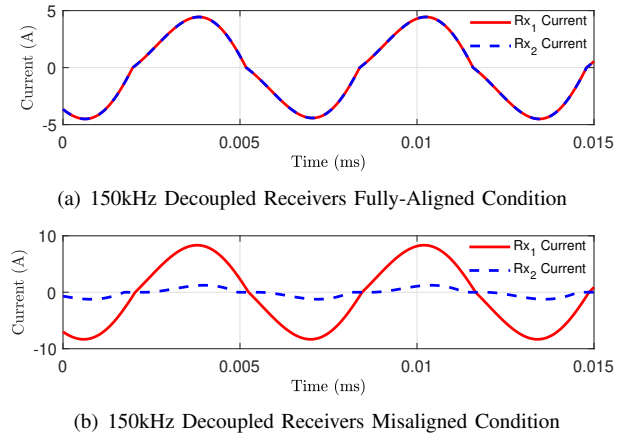

(a) 150kHz Decoupled Receivers Fully-Aligned Condition

(b) 150kHz Decoupled Receivers Misaligned Condition

Fig. 3. The change in the receiver currents for equal and different magnetic coupling.

A. Rectifier Effect and Load Sharing

In the previous section, the main phenomenon behind the unequal current sharing between Rx modules was explained. However, parallel connected Rx modules with a common DC bus (see Fig. 2) requires further analysis. The common DC voltage bus means that the voltage output of each Rx modules are equal. However, equal voltage doesn't imply equal power sharing. Actually, the reflected load resistance varies with coupling difference between the Tx and Rx modules. Since the system operates close to the design resonant frequency, the impedance of series connected LC resonant tank can be assumed to be zero. Then, it is possible to say that induced voltages at Rx modules can be conceivable as output voltage

as shown in (1) and (2). This is also valid for Tx and the equality is shown in (3).

$$V_{out} = j\omega M_1 I_p \quad (1)$$

$$V_{out} = j\omega M_2 I_p \quad (2)$$

$$V_{in} = -j\omega M_1 I_{s1} - j\omega M_2 I_{s2} \quad (3)$$

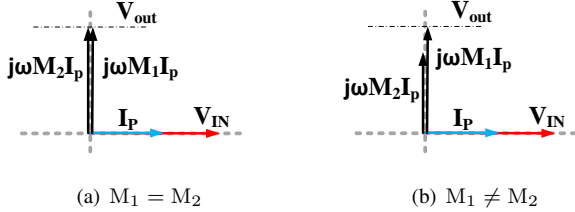First, let us consider the equal coupling case without any

(a) $M_1 = M_2$ (b) $M_1 \neq M_2$

Fig. 4. Rx side induced voltages for equal and unequal magnetic couplings.
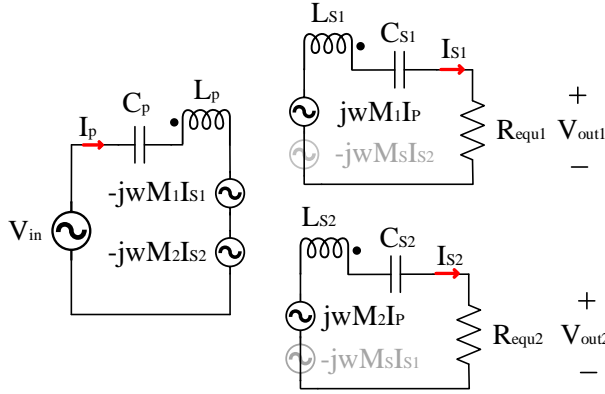
Fig. 5. Parallel Rx modules with and without cross-coupling.(Grayports show the cross-coupling components).

cross-coupling. The phasor diagram of the input and induced voltages at Rx's are shown Fig. 4. In this case, induced voltage of both Rx coils are equal to output voltage. Thus, the designed circuit operates as desired and Rx's share the power in equal. In the case of coupling mismatch, the Rx module with higher coupling has a higher induced voltage on its Rx side IPT coil, which is later rectified using the diode rectifier. The passive rectifier diodes on the less coupled module are reverse-biased and hence most of the power is transfered by a single module.

IV. Effect Of Receiver Cross-Coupling

One of the proposed methods is to introduce cross-coupling between the Rx modules as in Fig. 1. Then the first harmonic approximation (FHA) circuit representation of the system can be represented as in Fig. 5. Compared to the case with no cross-coupling there exists additional induced voltage components in the FHA circuit. The receiver with the larger coupling is named as the dominant Rx module and the other is named as recessive Rx module. When there is an unbalance between the module currents, the dominant module induces

EMF on the recessive Rx coil, which lags the dominant module current by 90°. The vectoral sum of these induced EMF components on the recessive module is hence higher, which helps to balance the current distribution. We can observe this effect using a phasor diagram of input and output voltages as shown in Fig. 6 for unequal coupling and negative coupling between Rx's. As shown in the phasor diagram, the receiver's output voltage is proportional to mutual inductance with the transmitter coil without cross-coupling. Although there exist small mutual inductance differences due to manufacturing, the slight voltage difference can be compensated by cross-coupling. Thus, the output voltages are equalized, and power unbalance between receivers is avoided by introducing cross-coupling. In Fig. 7, we observe the effect of cross-coupling on the receiver currents. The receiver currents are equal in the ideal case with cross-coupled as shown in Fig. 7(a). However, if the mutual inductances between Tx and Rx modules are not identical but comparable, we observe that one of the receivers is out of function as the mentioned previous section.In the Fig. 7(b), one of the receiver mutual inductance between the transmitter is smaller than the other as 10%, and cross-coupling is introduced as 70% of mutual inductance between receiver and transmitter. Then, we observe that the receiver currents are distributed almost equally.
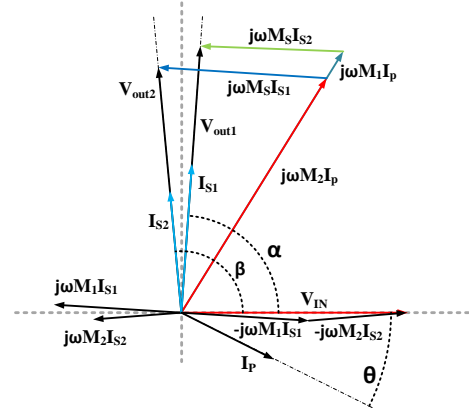

Fig. 6. Phasor diagram for common DC bus parallel connected Rx modules with cross-coupling.

Until now, the solution of load unbalance with cross-coupling was discussed. However, the required amount of cross-coupling is still undermined. Therefore, an analytical model is developed. Although additional cross-coupling is beneficial for better current sharing, the extra winding increases the overall system's resistive losses. Hence, a maximum allowable current unbalance needs to be chosen according to system needs, and the minimum cross-coupling should be used. In accordance with Fig. 5, the input and output voltages are defined as phasors as in Fig. 6 for the 1Tx-2Rx system with a resonant frequency of 150 kHz.

$$V_{out} = j\omega M_1 I_p + j\omega M_s I_{s2} \quad (4)$$

$$V_{out} = j\omega M_2 I_p + j\omega M_s I_{s1} \quad (5)$$

$$V_{in} = -j\omega M_1 I_{s1} - j\omega M_2 I_{s2} \quad (6)$$

(a) 150 kHz Cross-coupled Fully-Aligned Condition

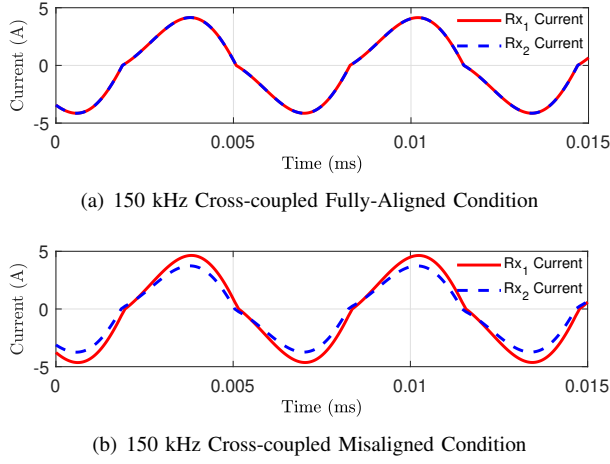(b) 150 kHz Cross-coupled Misaligned Condition

Fig. 7. Effect of cross-coupling on the Rx side current sharing

The magnitudes of the output voltages are equal but the phases depend on each Rx's current. Then, we can define the input parameters by considering FHA as in Fig. 6. The parameters are placed in (4,5, 6) and the equations (7,8,9) are obtained in the time domain.

$$V_{out} \sin(\omega t - \alpha) = \omega M_1 I_p \cos(\omega t - \theta) \\ + \omega M_s I_{s2} \cos(\omega t - \beta) \tag{7}$$

$$V_{out} \sin(\omega t - \beta) = \omega M_2 I_p \cos(\omega t - \theta) \\ + \omega M_s I_{s1} \cos(\omega t - \alpha) \tag{8}$$

$$V_{in} \sin(\omega t) = -\omega M_1 I_{s1} \sin(\omega t - \alpha) \\ - \omega M_2 I_{s2} \sin(\omega t - \beta) \tag{9}$$

After the conversion, the ortogonal set can be divided into two parts.

$$V_{out} \sin(\alpha) = -\omega M_1 I_p \cos(\theta) - \omega M_s I_{s2} \cos(\beta) \tag{10}$$

$$V_{out} \cos(\alpha) = \omega M_1 I_p \sin(\theta) - \omega M_s I_{s2} \sin(\beta) \tag{11}$$

$$V_{out} \sin(\beta) = -\omega M_2 I_p \cos(\theta) - \omega M_s I_{s1} \cos(\alpha) \tag{12}$$

$$V_{out} \cos(\beta) = \omega M_2 I_p \sin(\theta) - \omega M_s I_{s1} \sin(\alpha) \tag{13}$$

$$0 = -\omega M_1 I_{s1} \cos(\alpha) - \omega M_2 I_{s2} \cos(\beta) \tag{14}$$

$$V_{in} = -\omega M_1 I_{s1} \sin(\alpha) - \omega M_2 I_{s2} \sin(\beta) \tag{15}$$

Then, the system parameters are shown in Table I for a 1Tx-2Rx system. Also, the mutual inductances and desired receiver currents are used in the calculation as input. By considering the input parameters, the output voltage is calculated in (16) and the projection of input current on input voltages is calculated (17) by neglecting the losses for now.

$$V_{out} = (I_{s1} + I_{s2})R_L \tag{16}$$

$$I_{pf} = I_p(\theta) = \frac{V_{out}(I_{s1} + I_{s2})}{V_{in}} \tag{17}$$

For negative coupling between the Rx, it is known that dominant Rx current leads the input voltage in the range of 0 and 90 degree. Also, we know that recessive Rx current leads the input voltage in the range of 90 and 180 degree. The angles

of Rx currents with respect to the input voltage can be found by using equations. (14) and (15).

$$\delta = 180 - \arccos\left(\frac{V_{in}^2 - \omega^2 M_1^2 I_{s1}^2 - \omega^2 M_2^2 I_{s1}^2}{-2\omega^2 M_1 M_2 I_{s1}^2}\right) \tag{18}$$

$$\alpha = -\arctan\left(\frac{\omega M_1 I_{s1} + \omega M_2 I_{s1} \cos(\delta)}{\omega M_2 I_{s1} \sin(\delta)}\right) \tag{19}$$

$$\beta = \alpha - \delta \tag{20}$$

We can find the required cross-coupling (M_s) by using (10) and (11) or equations (12) and (13). In this equations, θ and M_s are unknown parameters. These equations can be reshaped in linear form by changing the parameters as $\tan(\theta)$ and M_s. The equation are brought $y = A^{-1}B$ form where A, B and y are shown in (21), (22) and (23).

$$A = \begin{bmatrix} \omega M_2 I_{pf} & \omega I_{s1} \cos(90 + \alpha) \\ 0 & \omega I_{s1} \sin(90 + \alpha) \end{bmatrix} \tag{21}$$

$$B = \begin{bmatrix} V_{out} \sin(\beta) \\ V_{out} \sin(\beta) - \omega M_2 I_{pf} \end{bmatrix} \tag{22}$$

$$y = \begin{bmatrix} \tan\theta \\ M_s \end{bmatrix} \tag{23}$$

The required cross coupling between Rx modules for a desired unbalance constraint can be calculated as shown (24).

$$M_s = \frac{V_{out} \sin(\beta) - \omega M_2 I_{pf}}{\omega I_{s1} \cos(90 + \alpha)} \tag{24}$$

In Table II, the input parameters, defined in Fig. 6 and calculated unknown output parameters are given. Inductance values and operation frequency are taken from the 1Tx-2Rx system design section. The scenario of a 5% difference between mutual inductances is discussed. For this scenario, the desired current distribution ratio is chosen as 70%, and the required cross-coupling is calculated as 0.167 ($M_s = 11.02$ μH).

TABLE II
CROSS-COUPLED ANALYTICAL INPUT PARAMETERS AND RESULTS

Input Parameters	Values	Unknown Parameters	Values
f	150 kHz	$V_{out}(rms)$	112.2 V
L_p	82 μH	α	76.6728°
L_s	66 μH	β	110.8°
M_1	14.71 μH	$I_p(rms)$	8.6170 A
M_2	13.97 μH	θ	19.54°
$V_{in}(rms)$	90 V	M_s	11.02 μH
$I_{s1}(rms)$	4.1 A		
$I_{s2}(rms)$	2.8 A		
R_L	20 Ω		

In Fig. 8, the simulation results for 0.167 cross-coupling coefficient are given. The receiver currents in the simulation are same as analytical calculations for the same cross-coupling. Thus, the analytical cross-coupling calculation is validated by simulation.
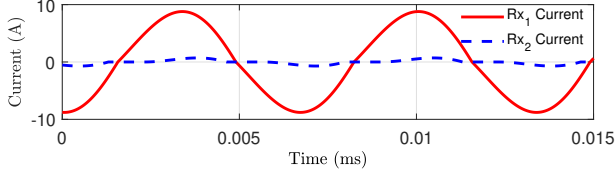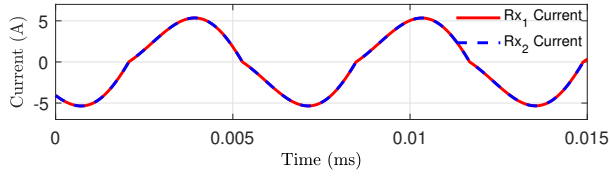
(a) 150 kHz Decoupled Condition ($I_{Rx1} = 6.2A_{rms}, I_{Rx2} = 0.5A_{rms}$)
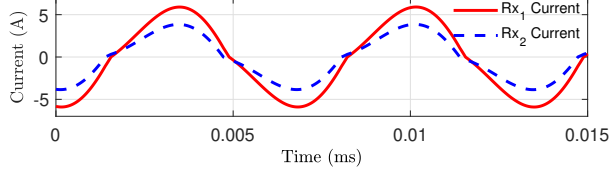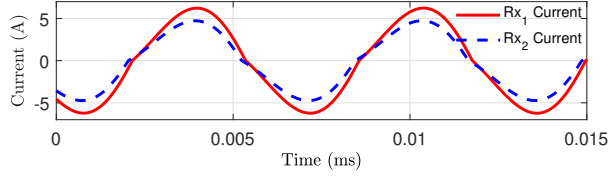

(b) 150 kHz Cross-Coupled Condition ($I_{Rx1} = 4.1A_{rms}, I_{Rx2} = 2.7A_{rms}$)

Fig. 8. Effect of cross-coupling on the current sharing for missaligned case.

(a) 135kHz Decoupled Receivers Fully-Alligned Condition

(b) 135kHz Decoupled Receivers Misalligned Condition

Fig. 9. Effect of detuning on the current sharing.

V. INTENTIONAL DE-TUNING OF RECEIVER SIDE RESONANT TANK

It is observed that increasing operating frequency (while keeping the resonant frequency same) results in a more balanced current sharing. However, as the operating frequency deviates further from the resonant frequency, the output voltage decreases and hence the power output reduces. The same current balancing effect can be achieved by intentional de-tuning of the receiver resonant tank. Feng *et al.* investigate a detuned 1Tx-1Rx system and the effect of changing coupling coefficient is analyzed with respect to power transfer variances [18]. In this section, the effect of Rx side detuning on current sharing is investigated for a 1Tx-2Rx system. Firstly, the analytical derivation is performed for a single Tx and single Rx system, and the effect of operation frequency and resonant tank frequencies are discussed. Secondly, a similar approach is used to analyze the effect of Rx side de-tuning for a 1Tx-2Rx system.

The first harmonic approximated circuit representation of 1Tx-1Rx system is presented in Fig. 10. The impedance of resonant tanks can be calculated by using resonant frequency, operation frequency and IPT coil inductances. The Tx and Rx resonant tank impedances are shown in (25) and (26). Then,
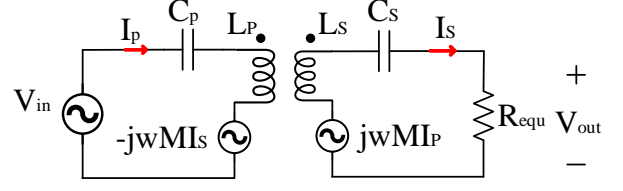

Fig. 10. First harmonic approximation of single transmitter single receiver IPT system.

the impedance matrix (27) can be solved for the transmitter and receiver currents as shown in (28) and (29).

$$jL_p\left(\frac{\omega_{op}^2 - \omega_p^2}{\omega_{op}^2}\right) = jL_p(\Delta\omega_p) \tag{25}$$

$$jL_s\left(\frac{\omega_{op}^2 - \omega_s^2}{\omega_{op}^2}\right) = jL_s(\Delta\omega_s) \tag{26}$$

$$\begin{bmatrix} V_{in} \\ 0 \end{bmatrix} = \begin{bmatrix} Z_p & j\omega M \\ j\omega M & -Z_s \end{bmatrix} \begin{bmatrix} I_p \\ I_s \end{bmatrix} \tag{27}$$

$$I_p = \frac{V_{in}(-L_s\Delta\omega_s + jR_L)}{L_pR_L\Delta\omega_p + j(M^2\omega_{op}^2 + L_pL_s\Delta\omega_p\Delta\omega_s)} \tag{28}$$

$$I_s = \frac{M\omega_{op}V_{in}}{L_pR_L\Delta\omega_p\Delta\omega_s + j(M^2\omega_{op}^2 + L_pR_L\Delta\omega_p)} \tag{29}$$

In conventional series-series IPT systems, the Tx and Rx side resonant tank frequencies are adjusted to be same in order to achieve independent operation under variable loads and magnetic coupling. However, in this paper it is shown that, for common DC bus parallel connected multi-Rx systems, the current sharing can be improved by intentional de-tuning. When both Tx and Rx frequencies are equal to each other, the Tx and Rx currents can be derived as in (30) and (31) respectively. Under this condition, the Rx current lags the Tx current by 90°.

$$I_p = \frac{V_{in}R_L}{M^2\omega_{op}^2} \tag{30}$$

$$I_s = \frac{-jV_{in}}{M\omega_{op}} \tag{31}$$

However, if the Rx resonant tank is de-tuned and operating frequency is kept at the resonant frequency of the Tx, the Tx and Rx currents can be derived as in (32) and (33).

$$I_p = \frac{V_{in}R_L}{M^2\omega_{op}^2} + \frac{jV_{in}L_s\Delta\omega_s}{M^2\omega_{op}^2} \tag{32}$$

$$I_s = \frac{-jV_{in}}{M\omega_{op}} \tag{33}$$

Therefore, detuning the Rx side results in leading or lagging Tx current while the Rx current stays same. If the resonant frequencies of the Rx's are chosen below the resonant frequency of the Tx side, the overall system resonant frequency will be above the resonant frequency of the transmitter and vice-versa. The analytical derivations can be expanded for 1Tx-2Rx

system shown in Fig. 5. The cross-coupling is ignored during derivation of Rx side detuning and rectifier can be modelled as variable load with common output voltage. The matrix equations for the system is shown in (34) and the receiver currents as in (35) and (36) are obtained.

$$\begin{bmatrix} V_{in} \\ 0 \\ 0 \end{bmatrix} = \begin{bmatrix} Z_p & j\omega M_1 & j\omega M_2 \\ j\omega M_1 & -Z_{s1} & 0 \\ j\omega M_1 & 0 & -Z_{s2} \end{bmatrix} \begin{bmatrix} I_p \\ I_{s1} \\ I_{s1} \end{bmatrix} \quad (34)$$

$$I_{s1} = \frac{jI_p M_1 \omega_{op}^2}{R_{L1}\omega_{op} + j(L_s^2(\omega_{op}^2 - \omega_s^2))} \quad (35)$$

$$I_{s2} = \frac{jI_p M_2 \omega_{op}^2}{R_{L2}\omega_{op} + j(L_s^2(\omega_{op}^2 - \omega_s^2))} \quad (36)$$

Although the load distribution of the modules are unknown, the magnitude of the voltages are equal as shown in (37). The extended formulation is shown in (38).

$$R_{L1} \mid I_{s1} \mid = R_{L2} \mid I_{s2} \mid \quad (37)$$

$$I_p M_1 \omega_{op}^2 R_{L1} \sqrt{R_{L1}^2 \omega_{op}^2 + L_s^4(\omega_{op}^2 - \omega_s^2)^2}$$
$$-I_p M_2 \omega_{op}^2 R_{L2} \sqrt{R_{L2}^2 \omega_{op}^2 + L_s^4(\omega_{op}^2 - \omega_s^2)^2} = 0 \quad (38)$$

When $\omega_{op} = \omega_s$, (39) can be derived. For this equation to hold, either R_{L1} or R_{L2} must go to infinity since $M_1 \neq M_2$.

$$I_p M_1 \omega_{op}^3 R_{L1} R_{L2} - I_p M_2 \omega_{op}^3 R_{L1} R_{L2} = 0 \quad (39)$$

However, if $\omega_{op} \neq \omega_s$ and with the assumption of a high quality factor, (40) can be obtained. Using the same assumptions, (38) can be written as in (41).

$$\sqrt{R_{L2}^2 \omega_{op}^2 + L_s^4(\omega_{op}^2 - \omega_s^2)^2} = L_s^2(\omega_{op}^2 - \omega_s^2) \quad (40)$$

$$I_p \omega_{op}^3 L_s^2(\omega_{op}^2 - \omega_s^2)(M_1 R_{L1} - M_2 R_{L2}) = 0 \quad (41)$$

By simplifying (41) and under the assumption that the Rx side is detuned and quality factor is high, the load distribution is inversely proportional to the mutual inductances ratio as shown in (42).

$$\frac{R_{L1}}{R_{L2}} = \frac{M_2}{M_1} \quad (42)$$

In summary, increasing operation frequency while having the same resonant tank at Tx and Rx, results in a better current distribution. However, as the frequency gets further into the inductive region, the power output decreases. If the Rx side resonant frequency is decreased, the maximum balancing that can be achieved as provided in (42). Moreover, with detuning operation at the resonant frequency is still achievable without any loss in the maximum power delivery capability. Again without any change, frequency control can be used to control the power output. The simulation result for normal and de-tuned receiver is given in the Fig. 9.

A major disadvantage of having detuned Rx side, is the variation in the resonant frequency for different loading and couplings. In the literature series-series topology is usually se-lected for its independence of resonant frequency for variable operating conditions. In our final 2Tx-4Rx design, the change in the reflected impedance is minimized. As the Rx modules

rotates, the Tx side the magnetic coupling with another Rx module while it decreases with the other Rx module. Therefore in our system, change in the resonant frequency is minimal.

VI. EXPERIMENTAL RESULTS

In Fig. 11, the 1Tx-2Rx system is presented. In the Tx side, there is a single full bridge converter while the other Rx circuits consists of passive diode full bridge rectifier connected in parallel to the same load. The system is similar to the system representation presented in Fig. 1. The Rx coils are under the ferrite shield and the Tx coils are under the Rx coils.
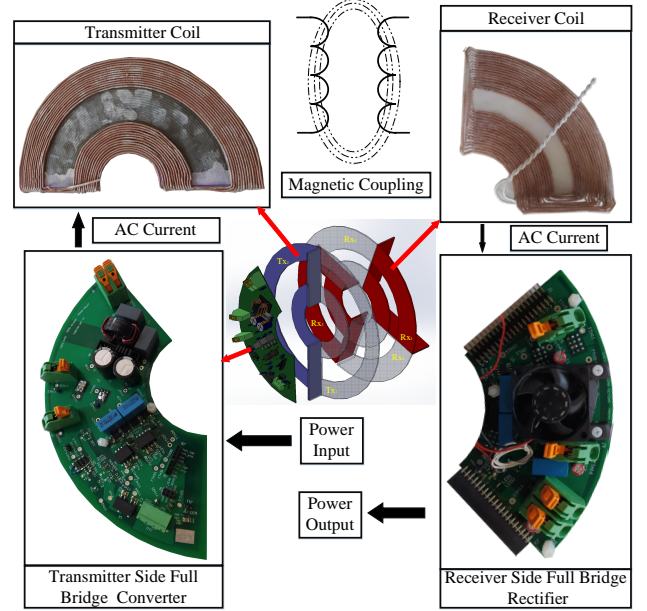

Fig. 11. Test setup illustration.

In this section two different alignment cases are investigated which are namely fully-aligned and missaligned. For the cross-coupled Rx modules the coupling is set to be $k_c = -0.15$ and for the detuned Rx side the resonant frequency of the Rx side is adjusted to be 135 kHz.
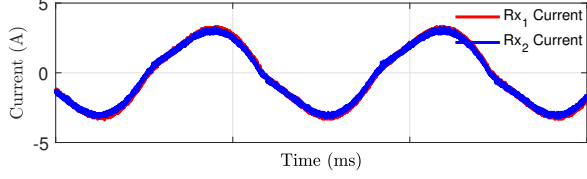
A. Fully-Aligned Case

The inductance matrice of the full-aligned system is pre-sented below in μH. Current distributions for decoupled/fully-tuned, decoupled/detuned and coupled/fully-tuned cases are presented in Fig. 12. Since the couplings between the Tx and Rx modules are very close, all Rx currents are nearly the same. However, since there exists small coupling and inductance differences due to manufacturing and testing the current balancing effect both proposed methods are already observable.
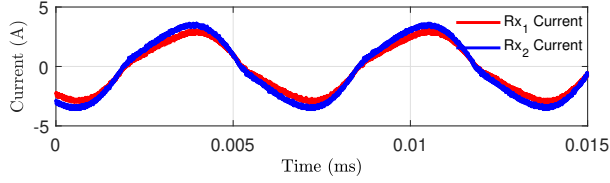
$$\begin{bmatrix} L_p & L_{p,s1} & L_{p,s2} \\ L_{p,s1} & L_{s1} & L_{s1,s2} \\ L_{p,s2} & L_{s2,s1} & L_{s2} \end{bmatrix} = \begin{bmatrix} 83.5 & 13.9 & 14.5 \\ 13.9 & 65.6 & -10.7 \\ 14.5 & -10.7 & 65.4 \end{bmatrix}$$
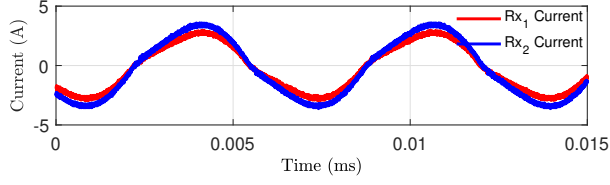
(a) 150 kHz Decoupled Receivers ($I_{Rx1} = 1.9A_{rms}, I_{Rx2} = 2.4A_{rms}$)

(b) 135 kHz Decoupled Receivers ($I_{Rx1} = 2.2A_{rms}, I_{Rx2} = 2.1A_{rms}$)

(c) 150 kHz Cross-Coupled Receivers ($I_{Rx1} = 2.0A_{rms}, I_{Rx2} = 2.4A_{rms}$)

Fig. 12. Rx current waveforms for fully-aligned case and different current balancing methods.

(a) 150 kHz Decoupled Receivers ($I_{Rx1} = 0.6A_{rms}, I_{Rx2} = 3.7A_{rms}$)

(b) 150 kHz Cross-Coupled Receivers ($I_{Rx1} = 1.5A_{rms}, I_{Rx2} = 2.8A_{rms}$)
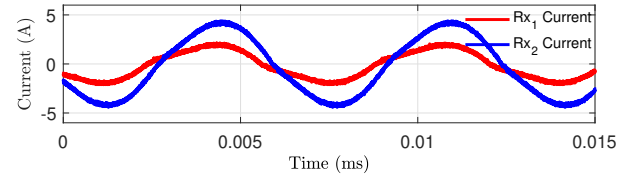
(c) 135 kHz Decoupled Receivers ($I_{Rx1} = 1.3A_{rms}, I_{Rx2} = 2.9A_{rms}$)

(d) 135 kHz Cross-Coupled Receivers ($I_{Rx1} = 1.8A_{rms}, I_{Rx2} = 2.5A_{rms}$)

Fig. 13. Effects of cross-coupling and detuning on the Rx side current distribution for the missaligned case.

B. Missaligned Case

In inductance matrice of the missaligned system is presented below in μH. The current balancing effect comparisons are first done for cross-coupling effect and detuning and finally for the combined balancing methods.

$$\begin{bmatrix} L_p & L_{p,s1} & L_{p,s2} \\ L_{p,s1} & L_{s1} & L_{s1,s2} \\ L_{p,s2} & L_{s2,s1} & L_{s2} \end{bmatrix} = \begin{bmatrix} 83.5 & 12.3 & 15.2 \\ 12.3 & 65.6 & -10.7 \\ 15.2 & -10.7 & 65.4 \end{bmatrix}$$
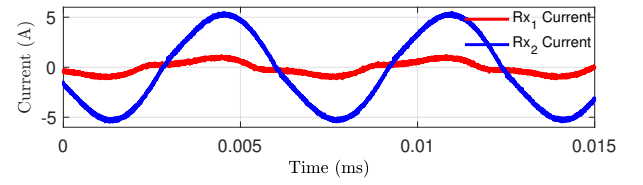
In Fig.13(b), the effect of cross-coupling for fully-tuned Rx side is presented. In Fig 13(c), the effect of detuning for no cross-coupling is presented. In Fig. 13(d), the combined current balancing effect of cross-coupled and detuned Rx modules is presented.
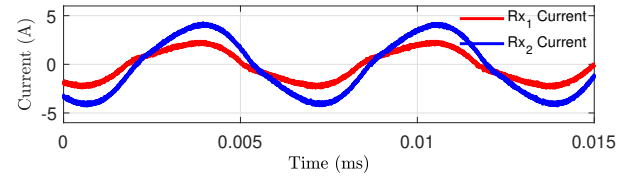
VII. DISCUSSION

In this section, firstly the experimental results will be discussed. Then the effect of proposed methods on the gain plots will presented. Let us define a current balance ratio(CBR) as in (43).

$$\text{CBR}(\%) = 100(1 - \frac{|\text{Current}_{Rx1} - \text{Current}_{Rx2}|}{\text{TotalCurrent}}) \quad (43)$$

Clearly, when both rms currents of each Rx modules are equal CBR is 100% which means that the currents are balanced. The rms current, CBR of each experiment, are presented in Table III. Also the current balancing improvement compared to decoupled and fully-tuned cases are included. According to Table III there is 55.8% improvement in the current sharing compared to decoupled/fully-tuned case. The Rx side coil AC resistance was measured as 0.3 Ω. The total Rx side coil ohmic
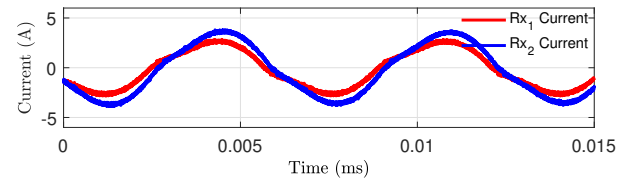
loss was also given in Table III. Although, the output power are the same for each experiment, the Rx side coil ohmic losses decreases with increased balancing due to reduced sum of $I_{s1}^2 R + I_{s2}^2 R + I_{s3}^2 R + I_{s4}^2 R$. The same is valid for Rx side rectifier diodes conduction losses.

Another important topic is the change in the overall system gain plots when cross-coupling and Rx side detunings are introduced. In Fig. 14 the gain plots for different current balancing methods are presented. The gain plots are obtained under fully-aligned condition. The initial system design resonant frequency was selected as 150 kHz as in Table I. As we introduce a negative cross-coupling the peak of gain plots shift to lower frequencies. The increase in the gain at resonant frequency is expected as the Rx coils also generate an induced EMF component on each other which further increases the output voltage as presented in Fig. 6. Detuning the Rx modules such that the resonant frequency is lower shifts the gain plot to higher frequencies. This is due to reflected impedance of the Rx side to the Tx side. The reflected impedance can be expressed as in (44).

$$Z_r = \frac{\omega^2 M_1^2}{R_{equ1} + j\omega L_s + \frac{1}{j\omega C_s}} + \frac{\omega^2 M_2^2}{R_{equ2} + j\omega L_s + \frac{1}{j\omega C_s}} \quad (44)$$
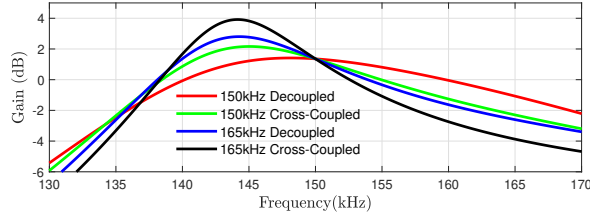
Decreasing the Rx side resonant frequency may have the same effect with increasing the series capacitor. At higher Rx side

TABLE III
CURRENT SHARING FOR MISSALIGNED DIFFERENT BALANCING METHODS AND IMPROVEMENTS

	Decoupled Rx/Fully Tuned	Cross-Coupled Rx/Fully Tuned	Decoupled Rx/De-tuned	Cross-Coupled Rx/De-tuned
Rx-1 Current	0.6 (A_{rms})	1.5 (A_{rms})	1.3 (A_{rms})	1.8 (A_{rms})
Rx-2 Current	3.7 (A_{rms})	2.8 (A_{rms})	2.9 (A_{rms})	2.5 (A_{rms})
Rx Copper Loss	4.21 (W)	3.03 (W)	3.05 (W)	2.85 (W)
CBR	27.9 (%)	69.7 (%)	61.9 (%)	83.7 (%)
Improvement		41.8 (%)	34 (%)	55.8 (%)
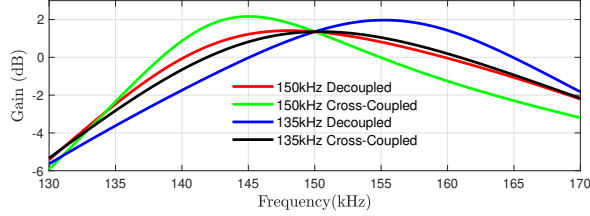
(a)

(b)

Fig. 14. $\frac{V_{out}}{V_{in}}$ gain plots for different current balancing methods.

capacitance, a higher frequency is needed for the resonance. A similar statement can be made for the opposite case where the Rx side resonant frequency is adjusted higher than the resonant frequency of the Tx side. In this case, the resonant frequency shifts even further into lower frequencies.

During the overall system design, first a maximum allowable current unbalance of 50% was selected. Solving the analytical model presented in the fourth section, resulted in either positive or negative cross-coupling with a magnitude of minimum 0.15. During the IPT coil finite element analysis , up curvature of IPT coils resulted in a much simpler negative cross-coupling adjustment without a significant change in the coil inductance. Moreover, with an up curvature coil design, a much uniform airgap flux density distribution was achieved due to elimination of the end windings. A much more detailed explanation of IPT coil design is beyond the scope of this paper. Then during the selection of Rx side detuning frequency 135 kHz was selected. Selection of 135 kHz did not only improve current sharing but also the gain plots of initial design (Decoupled/Fully-tuned) and final design are nearly overlapped.

VIII. SUMMARY

In this paper, two new current balancing method for common DC bus connected, modular, multi Tx and multi Rx IPT system was presented. The current balancing was achieved during the design procedure and without any extra DC-DC converters at the output. The analytical derivations are performed for 1Tx-2Rx case using first harmonic approxima-

tion. The first method is the introduction of cross-coupling which results in a 41% improvement in the current balancing. The second method is the intentional de-tuning of Rx side. By changing the resonant frequency 34% improvement was achieved. With the combination of these methods the CBR was increased to 83.7%. A similar improvement was also seen in the Rx side IPT coil ohmic losses where much more balanced current distribution resulted in a more efficient system.

REFERENCES

[1] G. A. Covic and J. T. Boys, "Modern trends in inductive power transfer for transportation applications," *IEEE Journal of Emerging and Selected Topics in Power Electronics*, vol. 1, no. 1, pp. 28–41, 2013.

[2] H. Hao, G. A. Covic, and J. T. Boys, "A parallel topology for inductive power transfer power supplies," *IEEE Trans. Power Electron.*, vol. 29, no. 3, pp. 1140–1151, 2014.

[3] S. Y. R. Hui and W. W. C. Ho, "A new generation of universal contactless battery charging platform for portable consumer electronic equipment," *IEEE Trans. Power Electron.*, vol. 20, no. 3, pp. 620–627, 2005.

[4] Y. Jang and M. M. Jovanović, "A contactless electrical energy transmission system for portable-telephone battery chargers," *IEEE Trans. Ind. Electron.*, vol. 50, no. 3, pp. 520–527, 2003.

[5] O. Knecht, R. Bosshard, and J. W. Kolar, "High-Efficiency Transcutaneous Energy Transfer for Implantable Mechanical Heart Support Systems," *IEEE Trans. Power Electron.*, vol. 30, no. 11, pp. 6221–6236, 2015.

[6] D. Patil, M. K. McDonough, J. M. Miller, B. Fahimi, and P. T. Balsara, "Wireless power transfer for vehicular applications: Overview and challenges," *IEEE Trans. Transport. Electrific.*, vol. 4, no. 1, pp. 3–37, March 2018.

[7] M. Fu, H. Yin, M. Liu, Y. Wang, and C. Ma, "A 6.78 mhz multiple-receiver wireless power transfer system with constant output voltage and optimum efficiency," *IEEE Trans. Power Electron.*, vol. 33, no. 6, pp. 5330–5340, 2018.

[8] V. B. Vu, V. T. Phan, M. Dahidah, and V. Pickert, "Multiple Output Inductive Charger for Electric Vehicles," *IEEE Trans. Power Electron.*, vol. 34, no. 8, pp. 7350–7368, 2019.

[9] M. Q. Nguyen, Y. Chou, D. Plesa, S. Rao, and J. C. Chiao, "Multiple-Inputs and Multiple-Outputs Wireless Power Combining and Delivering Systems," *IEEE Trans. Power Electron.*, vol. 30, no. 11, pp. 6254–6263, 2015.

[10] J. Pries, V. P. N. Galigekere, O. C. Onar, and G. J. Su, "A 50-kW Three-Phase Wireless Power Transfer System Using Bipolar Windings and Series Resonant Networks for Rotating Magnetic Fields," *IEEE Trans. Power Electron.*, vol. 35, no. 5, pp. 4500–4517, 2020.

[11] Y. Song, U. K. Madawala, D. J. Thrimawithana, and M. Vilathgamuwa, "Three-phase bi-directional wireless ev charging system with high tolerance to pad misalignment," *IET Power Electronics*, vol. 12, no. 10, pp. 2697–2705, 2019.

[12] D. Ahn and S. Hong, "Effect of coupling between multiple transmitters or multiple receivers on wireless power transfer," *IEEE Trans. Ind. Electron.*, vol. 60, no. 7, pp. 2602–2613, 2013.

[13] Z. Pantic, K. Lee, and S. M. Lukic, "Receivers for multifrequency wireless power transfer: Design for minimum interference," *IEEE Journal of Emerging and Selected Topics in Power Electronics*, vol. 3, no. 1, pp. 234–241, 2015.

[14] K. Colak, E. Asa, M. Bojarski, D. Czarkowski, and O. C. Onar, "A Novel Phase-Shift Control of Semibridgeless Active Rectifier for Wireless Power Transfer," *IEEE Trans. Power Electron.*, vol. 30, no. 11, pp. 6288–6297, 2015.

[15] M. Fu, C. Ma, and X. Zhu, "A cascaded boost-buck converter for high-efficiency wireless power transfer systems," *IEEE Transactions on Industrial Informatics*, vol. 10, no. 3, pp. 1972–1980, 2014.

[16] W. Song and A. Q. Huang, "Fault-tolerant design and control strategy for cascaded h-bridge multilevel converter-based statcom," *IEEE Trans. Ind. Electron.*, vol. 57, no. 8, pp. 2700–2708, Aug 2010.

[17] Y. Hu, G. Chen, Y. Liu, L. Jiang, P. Li, S. J. Finney, W. Cao, and H. Chen, "Fault-Tolerant Converter with a Modular Structure for HVDC Power Transmitting Applications," *IEEE Trans. Ind. App.*, vol. 53, no. 3, pp. 2245–2256, 2017.

[18] H. Feng, T. Cai, S. Duan, X. Zhang, H. Hu, and J. Niu, "A dual-side-detuned series–series compensated resonant converter for wide charging region in a wireless power transfer system," *IEEE Trans. Ind. Electron.*, vol. 65, no. 3, pp. 2177–2188, 2018.